Combining LIDAR and LADRC for intelligent pitch control of wind turbines

Chengzhen Jia [a, b], Lingmei Wang [a, b, *], Enlong Meng [b, f], Liming Chen [c], Yushan Liu [a, b], Wenqiang Jia [d], Yutao Bao [e], Zhenguo Liu [f]

[a] School of Computer and Information Technology, Shanxi University, Taiyuan, 030006, China
[b] Wind Turbine monitoring and Diagnosis Engineering Technology Research Center of Shanxi Province, Taiyuan, 030013, China
[c] School of Computing, Ulster University, Belfast, BT370QB, UK
[d] Taiyuan Heavy Industry New Energy Equipment Co., Ltd, Taiyuan, 030000, China
[e] Qinghai Green Power Distributed Energy Co., Ltd, Xining, 810001, China
[f] Automation Department, Shanxi University, Taiyuan, 030013, China

A R T I C L E   I N F O

A B S T R A C T

At present, most of the pitch control methods are based on PI controller, the pitch control system has poor disturbance resistance, and the research of variable parameter feedforward based on Light detection and ranging (LIDAR) and the Linear Active Disturbance Rejection controller (LADRC) composite control is rarely studied to reduce the blade root load, so this paper conceives a hybrid intelligent and adaptive pitch control approach to reduce a wind turbine generator speed fluctuation and its blade root load. Specifically, we combine the Radial Basis Neural Network and Finite Impulse Response filter (RBFNNFIR) based on LIDAR wind measurement. We then use a variable bandwidth of LADRC controller. Overall the approach enables and facilitates self-adaption and self-adjustment. We use Matlab *s*-function to call the multi-freedom mathematical wind turbine model based on FAST code, the composite intelligent control algorithm is established in Simulink. Initial results from the statistical analysis of the experiments under different turbulent wind conditions shows that the hybrid intelligent pitch control approach can reduce the generator speed fluctuation by about 40.8%, and the blade root max value of load moment by about 13.1%, compared with the baseline values of the traditional variable gain PI control algorithm.

1. Introduction

To support sustainable development, governments around the world have vigorously developed wind power to provide clean energy. In 2018, the global newly installed capacity of wind turbines is 51.3 GW. According to the prediction of the Global Wind Energy Council (GWEC), the global wind turbine installed capacity will increase by at least 55 GW per year by 2023. The new wind turbine installed capacity in China is 21.1 GW in 2018, and its total installed capacity still ranked first in the world. With the recent development of wind turbines [1], the inertial characteristics of wind turbines, e.g. the aerodynamic unbalanced load of wind turbine caused by wind shear and turbulence and the loading condition of turbine components such as blades handling in operation and maintenance has become increasingly complex, also become a significant challenge for pitch-speed control [2]. There are two problems in existing pitch-speed control algorithms: Firstly, the traditional anemometry device was installed at the end of the nacelle, and the measured wind speed is affected by blade rotation, so it could not represent the real wind speed near the hub. Fig. 1 shows the location of traditional wind measuring device, and the wind speed signal is not introduced into the pitch control above the rated wind speed. Secondly, the variable gain PI algorithm adopts a speed feedback method, as such, the pitching mechanism will not operate in time. As a result, the change of a generator speed lags behind the wind speed change, leading to large generator speed fluctuation. This is exactly the case when generator speed reaches the limit at which wind turbines will be shut down due to over-speed, which also causes the loss of power generation. With the development of LIDAR wind measurement technology in the field of wind power, the wind speed change of wind turbines can be

* Corresponding author. School of Computer and Information Technology, Shanxi University, No.92, Wucheng Street, Taiyuan City, Shanxi, China.
E-mail address: 13546468676@163.com (L. Wang).

Nomenclature

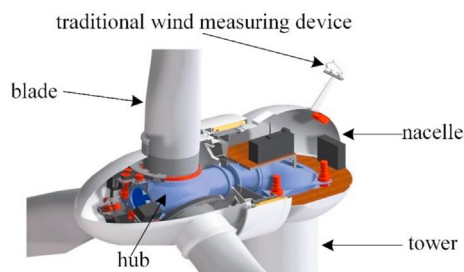|	
LIDAR	Light detection and ranging
LADRC	Linear Active Disturbance Rejection controller
RBFNN	Radial Basis Neural Network
FIR	Finite Impulse Response
ESO	Extended State Observer
PID	Proportional Integral Differential
GWEC	Global Wind Energy Council
FX-RLS	Filtered-x Recursive Least Squares
ZPET	Zero Phase Error Tracking
MPC	Model Predictive Control
GL	Germanischer Lloyd Industrial Services
CW	Continuous Wave
IEC	International Electrotechnical Commission
PL	Power-Law
IECKAL	The IEC Kaimal Model
IECVKM	The IEC Von Karman Isotropic Model
NWTCUP	The NREL National Wind Technology Center Model
GP_LLJ	The NREL Great Plains Low-Level Jet Model
SMOOTH	The Risø Smooth-Terrain Model
FF	Feedforward
FB	Feedback
J	Moment of inertia
P	Generator power
max	Maximum
min	Minimum
c	Chord length
v	Wind speed
λ	Tip speed ratio
r	The distance between the stress point and the blade root
C_t	Tangential force coefficient
C_n	Normal force coefficient
v_{LOS}	LIDAR measurement of wind speed in the sighting direction
$W(F,R)$	Space weighting function
v'_{LOS}	Wind speed at the focus
T_{pre}	Time of the wind reaches the hub
$\bar{v}$	Mean wind speed
z^{-1}	The unit delay
ϕ_i	Weighting coefficient of ith delay signal
α_1, α_2	Momentum factor in RBFNN
β	Actual output value of pitch actuator
β_{FB}	Control command value of pitch actuator
η	Learning rate
M_x	Force moment of blade root in the y direction
M_y	Force moment of blade root in the x direction
ρ	Air density
τ_β	The time constant of pitch actuator
T	Electromagnetic torque
std	Standard deviation
ω	Generator speed
w_0	ESO observation bandwidth

Fig. 1. Wind meter installation location diagram.

detected in advance. In this case, a feedforward controller can be designed to reduce the wind speed fluctuation influence on generator speed [3]. Therefore, an adaptive pitch control algorithm is helpful to the development of intelligent large-scale wind turbines.

At present, researchers have carried out extensive studies on wind turbine pitch control, including feedforward, model predictive control (MPC) based on LIDAR and generator speed feedback control technology. **In the field of LIDAR-based control technology**, Research in Ref. [4] analyzed and forecasted the application of LIDAR to wind turbine control comprehensively. Research in Ref. [5] analyzed the optimal distance of LIDAR measured wind speed, and the wind speed feedforward control based on LIDAR was used to reduce wind turbine load. Study in Ref. [6] proposed a FX-RLS adaptive feedforward control algorithm using LIDAR based on PI feedback pitch-speed control, and it had obvious advantages in speed tracking and power drop resistance comparing with zero phase error tracking (ZPET) feedforward control algorithm. Research in Ref. [7] proposed a feedback control strategy based on LIDAR wind measurement and considered the influence of wind

measurement error on the control effect. Study in Ref. [8] used the radial basis function neural network (RBF) algorithm based on the wind speed change measured by LIDAR to optimize the pitch angle and electromagnetic torque of wind turbines, and the purpose of optimal power generation and load reduction was achieved. Research in Refs. [9–11] proposed an MPC pitch control algorithm based on LIDAR using the linearized or nonlinear model of wind turbines. Research in Ref. [12] compared the pitch control effects of linear predictive and nonlinear predictive control based on LIDAR above rated wind speed in detail, which showed that the latter was better in maintaining stable speed. In summary, the LIDAR-based control technology always used the feedforward or MPC controller. However, the parameters adaptive change of feedforward controller was rarely studied, the MPC pitch controller always depends on the accurate linear mathematical model of wind turbines, but the mathematical model is not easy to obtain in actual engineering. **In terms of the feedback control of wind turbine generator speed**, Colombo et al. [13] used a robust sliding mode control technology to achieve stable control of the wind turbine's speed and power above the rated wind speed. Amirhossein et al. [14] proposed a fuzzy PID pitch controller which used the chaotic evolutionary optimization algorithm offline to optimize parameters of the PID controller. To address the delay characteristics of the pitch system, Gao et al. [15] designed a delay compensator to improve the original PI controller. Yuan et al. [16] designed an adaptive pitch controller by comparing the maximum wind energy capture and load reduction. Abdelbaky et al. [17] designed an incomplete fuzzy predictive offline pitch controller to adapt the wind speed fluctuation and the nonlinear model uncertainty. Ren et al. [18] proposed a nonlinear PI pitch controller based on state observer, the simulation results proved that the controller had good dynamic performance in terms of control power and load shedding. Lasheen et al. [19] used a variable-constrained time-varying predictive controller to reduce the system optimization calculation

time and enhance the adaptability of the pitch system to nonlinear characteristics. In Ref. [20], the chaotic evolutionary optimization algorithm was used to optimize the parameters of the RBF-based fractional-order PID pitch controller, which achieved better control performance and reduces the wind turbine load. The literature [21] used the robust control method to enhance the anti-interference performance of the pitch controller. Summarize the above research and study, the generator speed feedback control usually based on PI controller or sliding mode controller. The PI control algorithm uses the generator speed feedback to calculate the target command value of pitch actuator. However, the generator speed change lags behind the wind speed change, the pitch actuator cannot be acted upon according to the wind speed change timely, so it is not conducive to reducing generator speed fluctuation and the load of blade. The sliding mode controller may produce chattering when the state trajectory reaches the sliding mode surface. The existing composite pitch control algorithm is mostly combined with PI feedback control, but PI feedback controller has shortcoming. LADRC offers a new perspective where unmeasured disturbances and un-modeled dynamics can be estimated and compensated in real time by an ESO, thus addressing the drawbacks of PID controller [22,23]. In summary, in order to compensate for variations in parameters or dynamic behavior of wind turbines, and achieve a better control goal of disturbances rejection and robustness above the rated wind speed, the development of a composite intelligent pitch control algorithm based on LIDAR-assisted Feedforward and LADRC Feedback is quite necessary.

This paper proposes a novel composite intelligent adaptive pitch control approach based on LIDAR-assisted RBFNNFIR feedforward and the variable bandwidth LADRC controller, which enhances the robustness and disturbances rejection of the pitch control algorithm. The contributions of this paper include the following three aspects.

(1) We develop a RBFNN algorithm based on feedforward controller output and rotational speed error. The Jacobian matrix is designed to correct each coefficient of the FIR feedforward controller. This enables the feedforward controller to adjust the coefficient intelligently according to the wind condition and achieves the goal of robustness enhancing.

(2) According to the distribution of poles and zeros of the closed-loop system, the control parameters of the LADRC controller are adjusted. We use the look-up table method to realize the variation of LADRC observation bandwidth. A composite intelligent pitch control algorithmbased on RBFNNFIR feedforward and variable bandwidth LADRC controller is designed.

(3) Under the different wind conditions of step and turbulence, the comparative experimental analysis of four pitch control algorithms with PI, RBFNNFIR + PI, LADRC and RBFNNFIR + LADRC, shows that the proposed combined intelligent pitch control strategy can reduce the speed fluctuation and blade root load. Through the analysis of the experimental data under different amplitude steps and different turbulence models, the composite intelligent control strategy proposed in this paper has obvious advantages in terms of anti-interference and robustness.

The remaining of the paper is as follows. Section 2 introduces the mathematical model of the doubly-fed wind turbine and the mathematical model of LIDAR wind measurement in FAST software. Section 3 describes the proposed composite intelligent pitch control approach, including the RBFNNFIR feedforward control algorithm and variable bandwidth LADRC feedback control algorithm.

Section 4 outlines experiments, comparison and analysis between four different pitch control algorithms under different wind conditions. Section 5 summarizes the paper and discusses future research works.

2. The mathematical model of wind turbine and LIDAR wind measurement

A wind turbine is a complex dynamic nonlinear system, and its operating environment is intricate and varying. As a result, the load of main components of a wind turbine is dynamically changing, requiring a multi-freedom model to reflect its dynamic characteristics. The FAST wind turbine model has passed the certification of Germanischer Lloyd Industrial Services (GL), which can be used to simulate and verify the wind turbine control strategy [24]. The FAST software also integrates a LIDAR wind measurement module, which can measure wind speed change at different distances in front of the rotor. This is a foundation for the feedforward controller design based on wind speed.

2.1. Pitch control and load model of blade root

In this paper, a 5 MW horizontal axis three blades doubly-fed wind turbine model provided by FAST is adopted. The output of this model includes 40 variables, including time, wind speed measured by laser, rotating speed and power of the generator, force and moment at the root of the blade, etc. The model can selectively turn off unwanted degree of freedom. The FAST default model does not include the dynamic characteristics of the pitch actuator, so in this paper, a first-order inertia link is used to simulate the dynamic characteristics of the pitch actuator [25]. The expression is shown as formula 1.

$$\frac{\beta}{\beta_{FB}} = \frac{1}{\tau_\beta s + 1} \tag{1}$$

β is the actual output value of pitch actuator, β_{FB} indicates the control command value accepted by the pitch actuator. The pitch angle range is 0–90° and the maximum pitch rate is ±8°/s. When determining τ_β, the operation data of the actual electric pitch system is used, as shown in Fig. 2. The rotor diameter is 120 m, the sampling time of the data is 20 ms, and the approximate value of τ_β is obtained by the method of identifying. The time constant τ_β is about 0.2.

The study in this paper focuses on pitch control of the wind turbine operating above the rated wind speed, excluding the
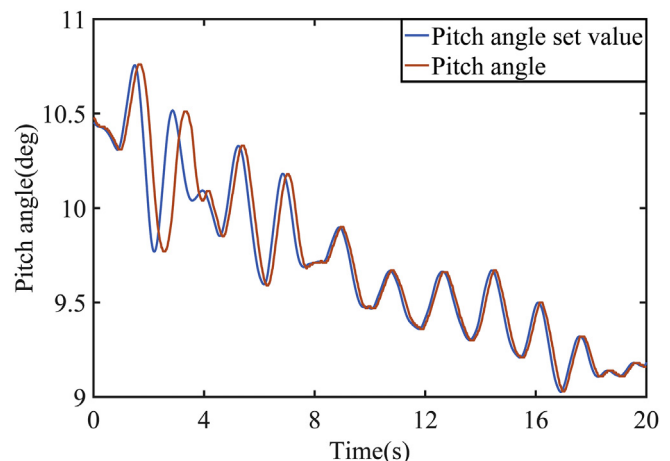

Fig. 2. The electric pitch system actual operation curve.

phases of start, stop and emergency stop. In this case, the generator power has reached the maximum value. In order to prevent the over-speeding of a wind turbine, the angle of its blade is changed to reduce the capture of wind energy, so as to maintain the constant power and speed of the wind turbine. Currently commercial pitch control usually adopts the variable gain PI algorithm based on speed feedback. When a speed deviation is caused by wind speed fluctuation, the PI controller makes the pitch actuator to act. The specific control block diagram is shown in Fig. 3.

The PI pitch control algorithm uses the speed error to generate the control quantity, which is not reasonable, because the given rated speed value can jump, and the wind turbine output speed is a slow changing variable, it is not reasonable to let the slowly changing quantity track the jumping quantity, and the introduction of speed error integral is easy to make the control link oscillate, so it is necessary to analyze the pitch of wind turbine in depth on the basis of dynamic characteristics.

A large number of literature studies shows that the torque of wind turbine is related to three variables of speed, pitch angle and wind speed [26,27]. Assuming that a wind turbine operates at the balance point A ($T_A, \omega_A, \beta_A, v_A$), the nonlinear function $T(\omega, \beta, v)$ can be obtained by Taylor expansion at the balance point A.

$$T = T_A + \alpha \Delta\omega + \xi \Delta\beta + \gamma \Delta v + h \tag{2}$$

In formula 2, $\alpha = \frac{\partial T}{\partial \omega}\big|_A$, $\xi = \frac{\partial T}{\partial \beta}\big|_A$, $\gamma = \frac{\partial T}{\partial v}\big|_A$, h represents the higher-order term in Taylor expansion. By combining formula 1 and formula 2, it can be concluded that:

$$\Delta\ddot{\omega} = \frac{\tau_\beta \alpha - J}{J\tau_\beta}\Delta\dot{\omega} + \frac{\alpha}{J\tau_\beta}\Delta\omega + \frac{\xi}{J\tau_\beta}\Delta\beta + \frac{\tau_\beta s + 1}{J\tau_\beta}(\gamma \Delta v + h) \tag{3}$$

As can be seen from the above formula, the pitch dynamic process of wind turbine can be regarded as a second-order system, and the input of the system is $\Delta\beta$, the system disturbance is $\frac{\tau_\beta s + 1}{J\tau_\beta}(\gamma \Delta v + h)$.

The change of pitch angle affects the generator speed and blade load of wind turbines. Blade load is the main source load of a wind turbine. In the mathematical modeling of blade load, a blade is usually divided into infinite blade elements along the radial direction based on the blade element momentum theory [28,29], then the aerodynamic load of the whole blade is obtained by integration. The force moment of each blade root in the x,y directions can be computed as follows respectively:

$$\begin{cases} M_x = \frac{1}{2}\rho \int cv^2 C_t(\lambda, \beta) r dr \\ M_y = \frac{1}{2}\rho \int cv^2 C_n(\lambda, \beta) r dr \end{cases} \tag{4}$$

For large megawatt wind turbines, reducing the main components load can help reduce production and maintenance costs, ensuring reliable operation of wind turbines. This has become a

major challenge of the wind turbine industry. The control technology is related to the dynamic load of key components closely, so combining advanced LIDAR wind measurement technology and developing intelligent pitch controlling technology to realize the load reduction and speed fluctuation suppression is the premise of LIDAR application in wind turbines successfully.

2.2. LIDAR wind measurement model

Current commercial laser radars include two main types: pulse and continuous wave (CW), both of which use the doppler frequency shift principle to measure wind speed [30]. Pulse laser radars are suitable for high-altitude measurements because of the high laser energy while CW laser radars are used for low-altitude measurements, which can collect wind data effectively under all weather conditions. This study uses a four-beam CW laser radar which has a 4 Hz sampling frequency, 30-degree angle between the laser beam and the horizontal plane is and a 25-degree angle with a vertical plane [31]. The reference coordinate system is based on the center of tower base, the downwind direction is the positive direction of x axis, and the direction of gravity is in the opposite direction of z axis. The specific wind measurement principle model is shown in Fig. 4.

The wind speed measured by a CW laser radar is not only the wind speed at the focus, but a mean wind speed in the direction of the laser beam, the space weighting function of the wind speed is $W(F,R)$. The wind speed is calculated in Equation (5) [32].

$$\begin{cases} v'_{LOS}(F) = \int_{-\infty}^{\infty} v_{LOS}(R) W(F,R) dR \\ W(F,R) = \frac{K_N}{R^2 + \left(1 - \frac{R}{F}\right)^2 R_R^2} \end{cases} \tag{5}$$

The laser radar collects the wind speed information at four points (v_1, v_2, v_3, v_4) in the same plane. The equivalent wind speed at the wind turbine hub height is calculated in Equation (6) [11].

$$v(t) = \frac{1}{4}\sum_{i=1}^{4} v'_{LOSi}(t)\lambda_i \tag{6}$$
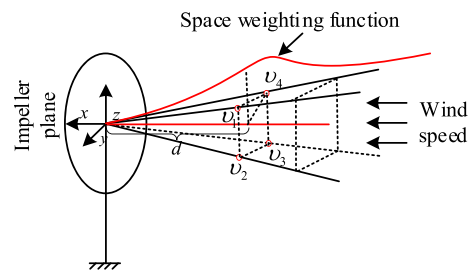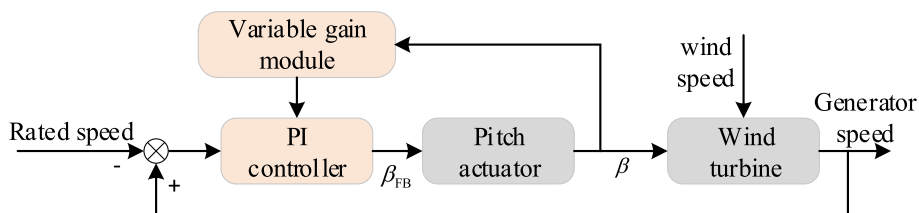
Fig. 4. LIDAR wind measurement diagram.

Fig. 3. Variable gain PI pitch control block diagram.

According to Taylor's frozen turbulence model, the advance time of wind speed can be approximately calculated in Equation (7).

$$T_{\text{pre}} \approx \frac{d}{\bar{\nu}} \tag{7}$$

We use the IECKAI turbulence model in the TurbSim module of the FAST software to generate wind speed data on an average of 17 m/s. Fig. 5 shows wind speed curve of four points ν_1(-50, 27.9, 33), ν_2(-50, 27.9, −33), ν_3(-50, −27.9, −33), ν_4(-50, −27.9, 33).

Because of the spatial weighting of laser wind radar measurements, the wind speed measured by LIDAR is equivalent to a low-pass filter for the actual wind speed, and the wind speed curve is relatively smooth [30,32]. It can be seen from Fig. 5 that the wind conditions of different measuring points are relatively different.

3. The composite intelligent pitch control algorithm

We conceive a composite intelligent pitch control algorithm, as shown in Fig. 6, to enable a wind turbine to adapt the changes of wind speed, thus reducing the generator's speed fluctuation. The approach uses the LIDAR to measure the wind speed at 50 m in front of the blade and the RBFNN method to estimate the error of the generator speed. It can then derive the speed of the generator several seconds in advance based on the wind speed change information. The Jacobian matrix will allow a FIR feedforward controller to adjust the FF's parameters accordingly. LIDAR measurement data and an adaptive pitch control algorithm is an inevitable requirement for the wind turbines towards intelligent development. In this paper, wind speed is measured by CW laser radar, it can provide wind speed change information. In parallel, the approach uses the variable bandwidth LADRC to make up for the traditional PI controller to support strong anti-interference and robustness. The combination of two modules forms a composite intelligent pitch control approach.

Feedforward and feedback composite controller has been widely used in industry [33,34], combining the advantages of both methods to enhance the anti-interference of control system. In Fig. 6, $G_1(s)$, $G_2(s)$, $G_3(s)$, $G_{FF}(s)$, $G_{FB}(s)$ represent the dynamic characteristics of LIDAR, pitch actuator, wind turbine, feedforward controller and feedback controller respectively. $D(s)$, $R(s)$, $Y(s)$ represent the disturbance, generator rated speed and generator speed of the wind turbine control system respectively. Equations (8)–(11) theoretically analyze the influence of feedforward controller on the system immunity and stability performance. The system output $Y(s)$ is calculated below.

$$Y(s) = \frac{G_{FB}(s)G_2(s)G_{FB3}(s)}{1 + G_{FB}(s)G_2(s)G_{FB3}(s)} R(s) + \frac{G_1(s)G_{FF}(s)G_2(s)G_{FB3}(s) + G_D(s)}{1 + G_{FB}(s)G_2(s)G_{FB3}(s)} D(s) \tag{8}$$

If the effect of a given input on the system is not considered, that is $R(s) = 0$, the relationship between system disturbance and output is shown as Equation (9).

$$\frac{Y(s)}{D(s)} = \frac{G_1(s)G_{FF}(s)G_2(s)G_{FB3}(s) + G_D(s)}{1 + G_{FB}(s)G_2(s)G_{FB3}(s)} \tag{9}$$

If there is no feedback link and only feedforward control, the relationship between disturbance and output is as follows.

$$\frac{Y(s)}{D(s)} = G_1(s)G_{FF}(s)G_2(s)G_{FB3}(s) + G_D(s) \tag{10}$$

As can be seen, the disturbance effect on the controlled quantity of the feedforward-feedback compound controller is $1/(1 + G_{FB}(s)G_2(s)G_{FB3}(s))$ of the simple feedforward controller.

The introduction of a feedforward controller will not affect the stability of the system, because the system characteristic equation has not changed, which can be computed as Δ.

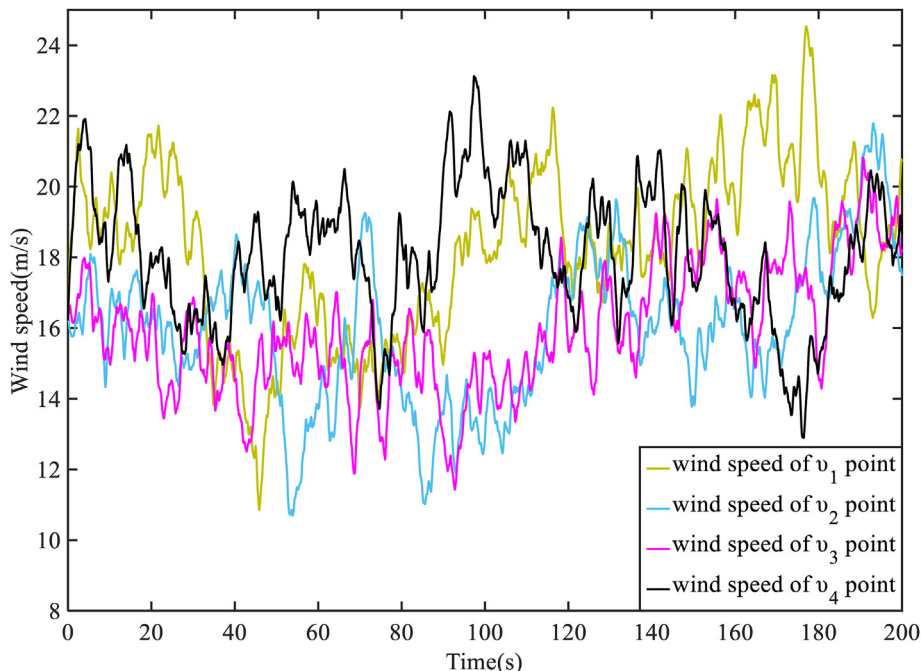$$\Delta(s) = 1 + G_{FB}(s)G_2(s)G_{FB3}(s) \tag{11}$$

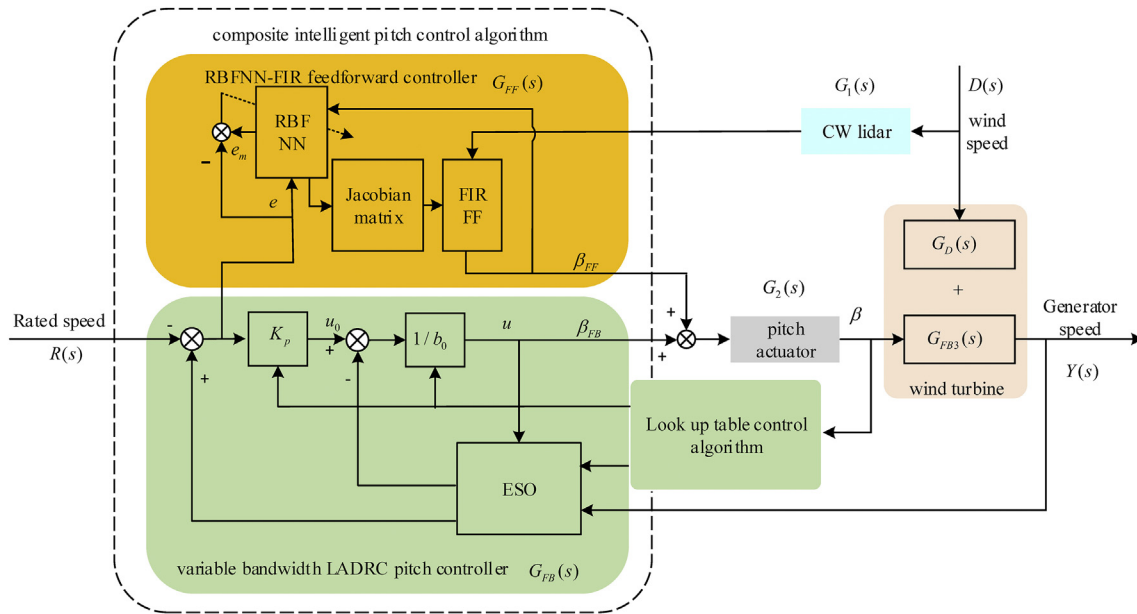**Fig. 5.** Wind speed curve at each point.

Fig. 6. The composite approach to intelligent pitch control.

3.1. LIDAR-assisted RBFNNFIR feedforward control algorithm

The FIR filter algorithm is widely used for feedforward control because of its stability [35,36]. Fig. 7 shows the basic principle of the FIR filter.

z^{-1} represents a unit delay and $\phi_i (i = 1, 2, \cdots N-1)$ is the weighting coefficient of i th delay signal, so the FIR output signal at k time is a linear weighted sum of inputs from the current time to the previous $N-1$ time, that is:

$$\beta_{FF}(k) = \sum_{i=0}^{N-1} \phi_i(k) \, v(k-i) \tag{12}$$

In order to enhance the robustness of a feedforward controller, it is necessary to adjust the coefficients of the filter dynamically, according to the variation of the generator speed fluctuation caused by wind fluctuation. We propose a new method RBFNNFIR to realize the adaptive adjustment of the feedforward controller. The production of RBFNN has a strong biological background. It is a feedforward neural network including an input layer, an output layer, and only one hidden layer. It imitates the neural network structure of local adjustment and mutual coverage of human brain. It can approach any nonlinear function with any precision. The relationship between the input layer and the hidden layer is a nonlinear transformation, but the hidden layer and output layer are linear. The operation relationship between neurons in each layer of RBFNN is shown in Fig. 8.

In RBFNN, the input vector of the network is $X = [x_1, x_2, \cdots, x_n]^T$, the radial basis vector of the nodes in the hidden
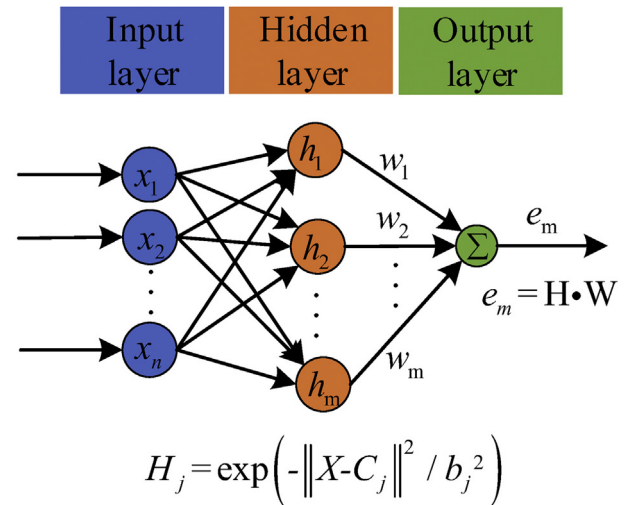

$$H_j = \exp\left(-\|X\text{-}C_j\|^2 / b_j^2\right)$$
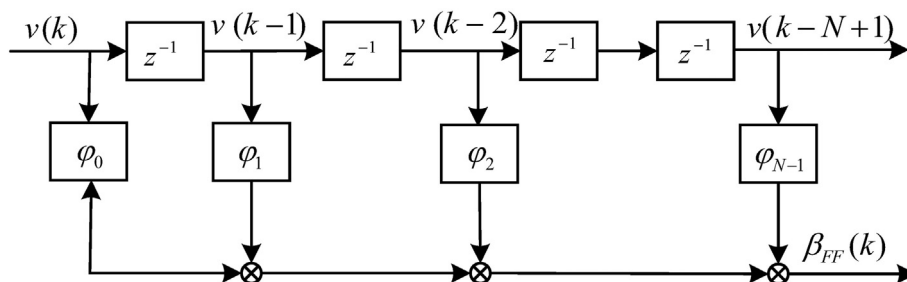
Fig. 8. Principle diagram of RBFNN.

Fig. 7. Principle diagram of FIR filter.

layer is $h = [h_1, h_2, \cdots, h_m]^T$, which is the Gaussian function. The center vector of the jth node in the hidden layer is $C_j = [C_{j1}, C_{j2}, \cdots, C_{jm}]^T$, the node base width vector is $b = [b_1, b_2, \cdots, b_m]^T$, the weight vector is $w = [w_1, w_2, \cdots, w_m]^T$, the output of the identification network at k time is $e_m(k)$, and the output of RBFNN is shown as Equation (13).

$$e_m(k) = w_1 h_1 + w_2 h_2 + \cdots + w_m h_m \tag{13}$$

The RBFNN performance index function is shown in Equation (14).

$$E(k) = \frac{1}{2}(e(k) - e_m(k))^2 \tag{14}$$

The gradient descent method is used to iterate the parameters of RBFNN, in order to make the search process converge to the global minimum, two momentum terms are introduced which includes the coefficients variation at two moments before k time, are shown as Equation (15)–(19).

$$w_j(k) = w_j(k-1) + \eta(e(k) - e_m(k))h_j + \alpha_1(w_j(k-1) - w_j(k-2)) + \alpha_2(w_j(k-2) - w_j(k-3)) \tag{15}$$

$$\Delta b_j = (e(k) - e_m(k))w_j h_j \frac{\|X - C_j\|^2}{b_j^2} \tag{16}$$

$$b_j(k) = b_j(k-1) + \eta \Delta b_j + \alpha_1(b_j(k-1) - b_j(k-2)) + \alpha_2(b_j(k-2) - b_j(k-3)) \tag{17}$$

$$\Delta c_{ji} = (e(k) - e_m(k))w_j h_j \frac{x_j - c_{ji}}{b_j^2} \tag{18}$$

$$c_{ji}(k) = c_{ji}(k-1) + \eta \Delta c_{ji} + \alpha_1(c_{ji}(k-1) - c_{ji}(k-2)) + \alpha_2(c_{ji}(k-2) - c_{ji}(k-3)) \tag{19}$$

The momentum factor in a reasonable range can accelerate the convergence speed of the neural network, and the unreasonable value will cause neural network random oscillation when it converges to a stable point. References [37,38] use a large number of experimental data to verify the momentum factor technology advantages on learning speed and training accuracy of the neural network, so it is necessary to take a reasonable value for α_1 and α_2, and their value range is general 0−1. The structure of the RBFNNFIR feedforward controller is depicted in the yellow part in Fig. 6.

The output of RBFNN is the speed error estimation. RBFNN can adjust the parameters on-line according to network identification performance index function shown as equation (16). At the same time, it can give the parameter adjustment algorithm of FIR feedforward controller according to the Jacobian matrix. The control goal of feedforward controller is to ensure that the generator speed error is minimum in case of wind speed fluctuation disturbance, so the performance index function is taken as:

$$J = \frac{1}{2}e(k)^2 \tag{20}$$

The sensitivity of speed error to the control input of feedforward controller is called Jacobian information, and its value can be approximated by RBFNN, take the first input of RBFNN as $\beta_{FF}(k)$, that is $x_1 = \beta_{FF}(k)$, the Equation is as follows.

$$\frac{\partial e(k)}{\partial \beta_{FF}(k)} \approx \frac{\partial e_m(k)}{\partial \beta_{FF}(k)} = \sum_{j=1}^{m} w_j h_j \frac{c_{1j} - x_1}{b_j^2} \tag{21}$$

The output increment of a feedforward controller is:

$$\Delta \beta_{FF}(k) = \beta_{FF}(k) - \beta_{FF}(k-1) = \sum_{i=0}^{N-1} \phi_i(k)(v(k-i) - v(k-1-i))$$
$$= \sum_{i=0}^{N-1} \phi_i(k)\Delta v(k-i) \tag{22}$$

The gradient descent method is used to adjust the parameters of the FIR feedforward controller. Equation (23)–(26) forms Jacobian matrix.

$$\Delta \phi_0(k) = -\eta_0 \frac{\partial J}{\partial \phi_0} = -\eta_0 \frac{\partial J}{\partial e} \frac{\partial e}{\partial \phi_0} \approx -\eta_0 \frac{\partial J}{\partial e} \frac{\partial e_m}{\partial \beta_{FF}} \frac{\partial \beta_{FF}}{\partial \phi_0}$$
$$= -\eta_0 e(k) \frac{\partial e_m}{\partial \beta_{FF}} \Delta v(k) \tag{23}$$

$$\Delta \phi_1(k) = -\eta_1 \frac{\partial J}{\partial \phi_1} = -\eta_1 \frac{\partial J}{\partial e} \frac{\partial e}{\partial \phi_1} \approx -\eta_1 \frac{\partial J}{\partial e} \frac{\partial e_m}{\partial \beta_{FF}} \frac{\partial \beta_{FF}}{\partial \phi_1}$$
$$= -\eta_1 e(k) \frac{\partial e_m}{\partial \beta_{FF}} \Delta v(k) \tag{24}$$

......

$$\Delta \phi_{N-1}(k) = -\eta_{N-1} \frac{\partial J}{\partial \phi_{N-1}}$$
$$= -\eta_{N-1} \frac{\partial J}{\partial e} \frac{\partial e}{\partial \phi_{N-1}} \approx -\eta_{N-1} \frac{\partial J}{\partial e} \frac{\partial e_m}{\partial \beta_{FF}} \frac{\partial \beta_{FF}}{\partial \phi_{N-1}}$$
$$= -\eta_{N-1} e(k) \frac{\partial e_m}{\partial \beta_{FF}} \Delta v(k-N+1) \tag{25}$$

$$\phi_i(k) = \phi_i(k-1) + \Delta \phi_i(k) \quad i = 1, 2, \cdots \cdot n \tag{26}$$

The negative gradient direction is used to determine the new search direction of each iteration, and each iteration can gradually reduce the parameters $\phi_0, \phi_1, \cdots \cdot, \phi_{N-1}$ to be optimized. $\eta_0, \eta_1, \cdots \cdot, \eta_{N-1}$ represent the learning rate of the feedforward controller coefficient.

3.2. Variable bandwidth LADRC feedback control algorithm

Han et al. [39] proposed and revisited the ADRC control technology in 1960, which can compensate for the uncertainty disturbance, and solves the problem of the traditional PI control algorithm. In order to facilitate the engineering application, Gao et al. [40] proposed the Linear Active Disturbance Rejection controller (LADRC). The LADRC controller does not depend on the accurate mathematical model, and can estimate and compensate the system disturbance in time through ESO. In this paper, we apply one order LADRC algorithm to the wind turbine pitch controlling above the rated wind speed. Due to the nonlinearity of wind turbine, and in order to enhance the control performance of the LADRC controller, we propose a new variable parameter LADRC pitch control strategy. The structure of the controller is shown in the green part in Fig. 6.

Let $y = \Delta \omega = x_1$, $u = \Delta \beta_{FF}$, the state space of Equation (3) can be

expressed as:

$$\begin{cases} \dot{x}_1 = x_2 \\ \dot{x}_2 = D(x_1 , x_2 , f) + b_0 u \\ y = x_1 \end{cases} \tag{27}$$

The control rate of a pitch controller in Fig. 6 is:

$$u = \frac{u_0 - z_2}{b_0} \tag{28}$$

By combining Equations (27) and (28), we can obtain:

$$\ddot{y} = (D - z_2) + u_0 \tag{29}$$

$D(x_1 , x_2 , f)$ delegates the total disturbance inside and outside of the system. On this basis, an ESO was designed. The mathematical formula of the ESO is shown as Equation (30).

$$\begin{cases} \dot{z}_1 = z_2 + \beta_1(y - z_1) + b_0 u \\ \dot{z}_2 = \beta_2(y - z_1) \end{cases} \tag{30}$$

z_1 and z_2 denote the estimators of y and D respectively. When β_1 and β_2 is appropriately adjusted, y and D can be tracked accurately, and Equation (29) can be simplified as:

$$\ddot{y} \approx u_0 \tag{31}$$

The object can be regarded as two integral objects connected in series after compensation, and the proportional controller is designed for control:

$$u_0 = k_p(r - y) \tag{32}$$

The parameters that need to be adjusted in the LADRC controller are K_p, b_0, β_1 and β_2. As there is a relationship between β_1, β_2 and the bandwidth of ESO as shown as Equation (33) [34], the LADRC controller actually has two parameters to be set, namely b_0 and w_0.

$$\begin{cases} \beta_1 = 2w_0 \\ \beta_2 = {w_0}^2 \\ K_p = 2w_c \\ w_0 = 0.125w_c \end{cases} \tag{33}$$

w_0 represents the observation ability of an ESO. w_c is the control bandwidth of the controller. Because the controlled object is simplified as a second-order system, the model of the controlled object can be expressed as follows:
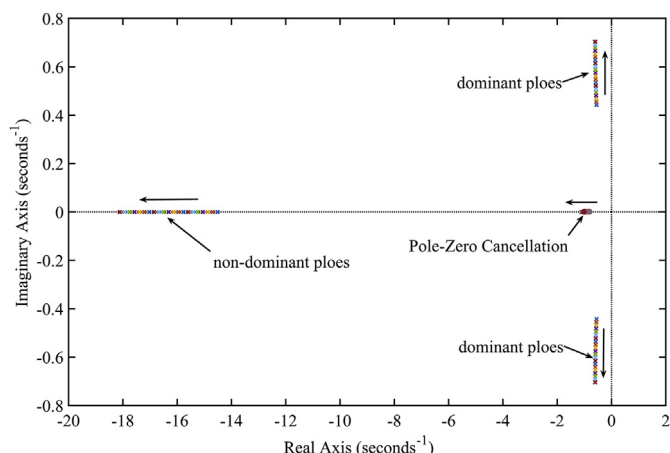

Fig. 9. The system poles and zeros distribution.

Table 1
The LADRC controller parameters under different wind speed.

Wind speed (m/s)	Pitch angle (deg)	K_p	b_0	w_0	damping ratio
12	3	11.52	405	0.72	0.707
14	8	12.48	195	0.78	0.708
16	11.5	14.56	245	0.91	0.709
18	14.5	17.12	320	1.07	0.706
20	17	19.04	450	1.19	0.706
22	19.5	20.32	750	1.27	0.706
24	22	28.16	400	1.76	0.706

$$y(s) = \frac{K}{(\tau_1 s + 1)(\tau_2 s + 1)} u(s) \tag{34}$$

Through the experiment of open-loop pitch angle perturbation under different wind speeds, the transfer function reflecting the dynamic characteristics of the controlled object is obtained. Combined with Equations (30) and (32)–(34), the closed-loop transfer function of the control system can be expressed as follows:

$$\begin{cases} \dfrac{y(s)}{r(s)} = \dfrac{A_2 s^2 + A_1 s + A_0}{B_4 s^4 + B_3 s^3 + B_2 s^2 + B_1 s + B_0} \\ A_0 = KK_p w_0^2 \\ A_1 = 2KK_p w_0 \\ A_2 = KK_p \\ B_0 = KK_p w_0^2 \\ B_1 = 2KK_p w_0 + 2b_0 w_0 + K_p b_0 + Kw_0^2 \\ B_2 = 2b_0 w_0(\tau_1 + \tau_2) + K_p b_0(\tau_1 + \tau_2) + b_0 \\ B_3 = 2b_0 w_0 \tau_1 \tau_2 + K_p b_0 \tau_1 \tau_2 + b_0(\tau_1 + \tau_2) \\ B_4 = b_0 \tau_1 \tau_2 \end{cases} \tag{35}$$

It can be seen from Equation (35) that under the specific wind speed, the change of w_0 and b_0 will affect the distribution of dominant poles of the closed-loop system, and the value of b_0 can be obtained from the open-loop identification model of the system. Therefore, the other control parameter w_0 can be determined according to the change of the dominant pole. When the wind speed is 16 m/s, the system poles and zeros distribution are shown in Fig. 9, the parameter w_0 is changing from 0.8 to 1.

The observer bandwidth w_0 is obtained by theoretical analysis of the distribution of zeros and poles in the closed-loop system with a damping ratio about 0.707. Thus, the control parameters is obtained as shown in Table 1.

The value of b_0 and w_0 can be looked up on table by condition in actually wind turbine running, so the parameters can change along with the pitch angle, thus avoiding the weak adaptability of fixed parameters. The linear interpolation method is used for the adjacent two points. Some of the tuned parameters have been modified slightly due to the unstable control of the parameters under some working conditions. Finally, we get the control curve of the parameters, as shown in Fig. 10.

4. Experiment and data analysis

FAST and GH Bladed are two wind turbine simulation software toolkits widely used in the wind energy industry [41,42]. As GH Bladed is commercially licensed with high cost, this paper used
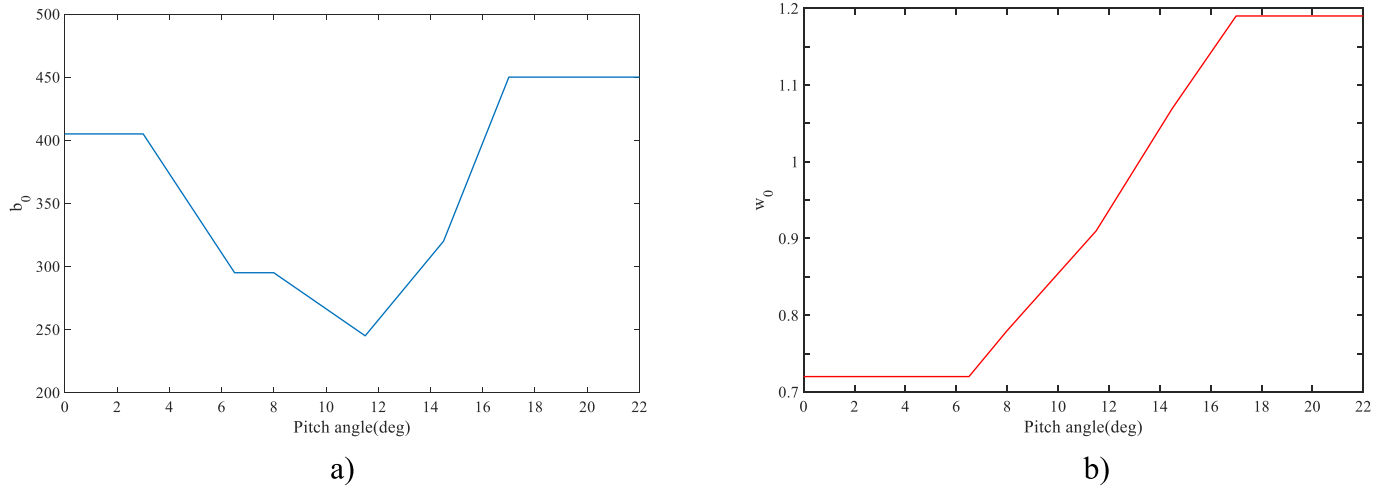
Fig. 10. Changing curves of parameters: a) Changing curve of b_0; b) Changing curve of w_0.

Table 2
Main parameters of 5 MW wind turbine.

Parameter	Value
Rated power	5 MW
Rotor Diameter	126 m
Tower height	87.6 m
Cut in wind speed, rated wind speed	3 m/s, 11.4 m/s
Rotor weight	110000 kg
Nacelle weight	240000 kg
Tower weight	347460 kg
Minimum speed	670 rpm
Rated speed	1173.7 rpm
Maximum wind energy utilization factor	0.482
Tip speed ratio	7.55
Gearbox ratio	97:1
Generator efficiency	94.4%

FAST for testing and evaluation. FAST is an open-source software developed by the National Renewable Energy Laboratory (NREL) of the United States for the comprehensive calculation and simulation of wind turbine performance and load. It provides a Matlab/Simulink interface to support Simulink for building wind turbine control strategies. The main parameters of 5 MW doubly-fed wind turbine adopted in this paper are shown in Table 2.

We use Simulink to build four pitch control algorithm including PI, RBFNNFIR + PI, LADRC and RBFNNFIR + LADRC control, and then develop joint simulation with FAST to test and evaluate the performance of the proposed composite intelligent pitch control approach.

4.1. Experimental analysis of speed control and load bearing

Pitch control is a mechanism to ensure the stability of generator speed when a wind turbine operates above the rated wind speed. In order to verify the superiority of the RBFNNFIR + LADRC pitch control strategy proposed in this paper, the control effects of four pitch control strategies are compared and analyzed under the different wind conditions including step and turbulent. The main parameters of the controller setting are shown in Table 3. The LIDAR measured wind speed data is at 50 m in front of the blade, and its sampling frequency is 4 Hz.

For the step wind condition, it is assumed that the time for wind at 50 m ahead of the rotor takes 3 s to reach, and the wind speed does not change. The step change of wind speed is shown in Fig. 11 (a), and the comparison curve of speed, power, pitch angle and blade root load moment are shown in Fig. 11 (b)–(f).

As can be seen in Fig. 11 (b)–(c), the RBFNNFIR + LADRC composite intelligent control approach can reduce the speed and power fluctuation, because both PI and LADRC controllers with feedforward control can make the pitch angle act in advance, as shown in Fig. 11 (d). Compared with PI controller, the LADRC controller has remarkable effect in reducing generator speed and power fluctuation, and can reduce the overshoot of pitch angle and make pitch angle track steady target value rapidly as well. Under the four control strategies, the blade root moment in the x direction is not significantly different, because it is affected by the force in the y direction and the gravity of the blade itself, and these two factors have not changed. For the blade root moment in y direction, both PI and LADRC controllers with feedforward control can reduce the maximum change moment and can also enter the stable state faster when the wind speed changes, meanwhile, LADRC controllers can achieve better control results than PI controller, as shown in Fig. 11 (f).

The step wind speed experiment can help us to obtain the time-domain dynamic response index of the pitch control system, which is convenient for us to debug the parameters of the controller, but it is an ideal state. In order to get closer to the actual wind situation, we did the experiment with a turbulent wind, as shown in Fig. 12

Table 3
Main parameters of controller setting.

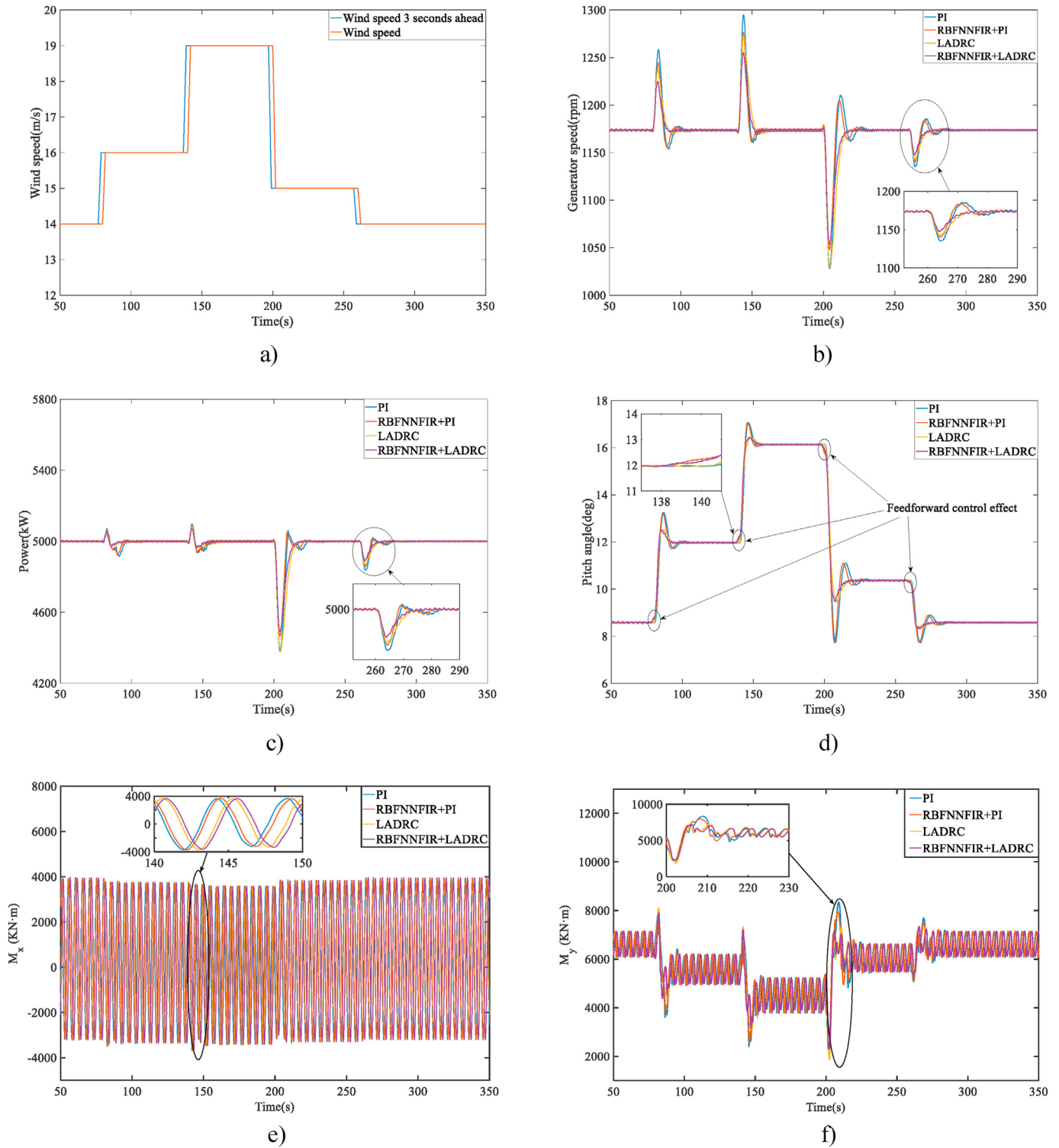| Controller	Parameter value
PI	$K = 0.01882681 \times G(\theta)$; $I = 0.008068634 \times G(\theta)$
	$G(\theta) = \dfrac{1}{1 + \dfrac{\theta}{0.1099965}}$
LADRC	$b_0 = f_1(\beta)$ (Fig. 10a); $w_0 = f_2(\beta)$ (Fig. 10b)
RBFNNFIR	$m = 7$; $\eta = 0.5$; $\alpha_1 = 0.05$; $\alpha_2 = 0.01$; $C_{ini} = 0.1$; $b_{ini} = 0.2$; $w_{ini} = 5$; $\phi_{ini} = 0.0004$; $\eta_\phi = 0.0001$

Fig. 11. Comparison of four control strategies under step wind speed: a) Step wind speed curve; b) Generator speed curve; c) Power curve; d) Pitch angle curve; e) Bladeroot moment M_x curve; f) Bladeroot moment M_y curve.

(a), the curve of speed, power, pitch angle and blade root load moment are shown in Fig. 12 (b)–(f).

Statistical analyses show that, the wind turbine speed variance for the four control strategies are 34.56, 28.48, 29.12, 22.26 respectively, and the power variances are 98.86, 88.59, 96.26, 85.34. Compared with the traditional PI control, the RBFNNFIR + LADRC

pitch controller can reduce the speed variance by 35.6% and the power variance by 13.6%. The mean values of wind turbine blade root load moment in x direction are 176.4, 174.1, 173.3, 172.1, and the variances are 2526, 2524, 2520, 2520, respectively. The mean values of load moment in y direction are 5081, 5084, 5057, 5063, and the variances are 1872, 1842, 1821, 1791, respectively. Compared with
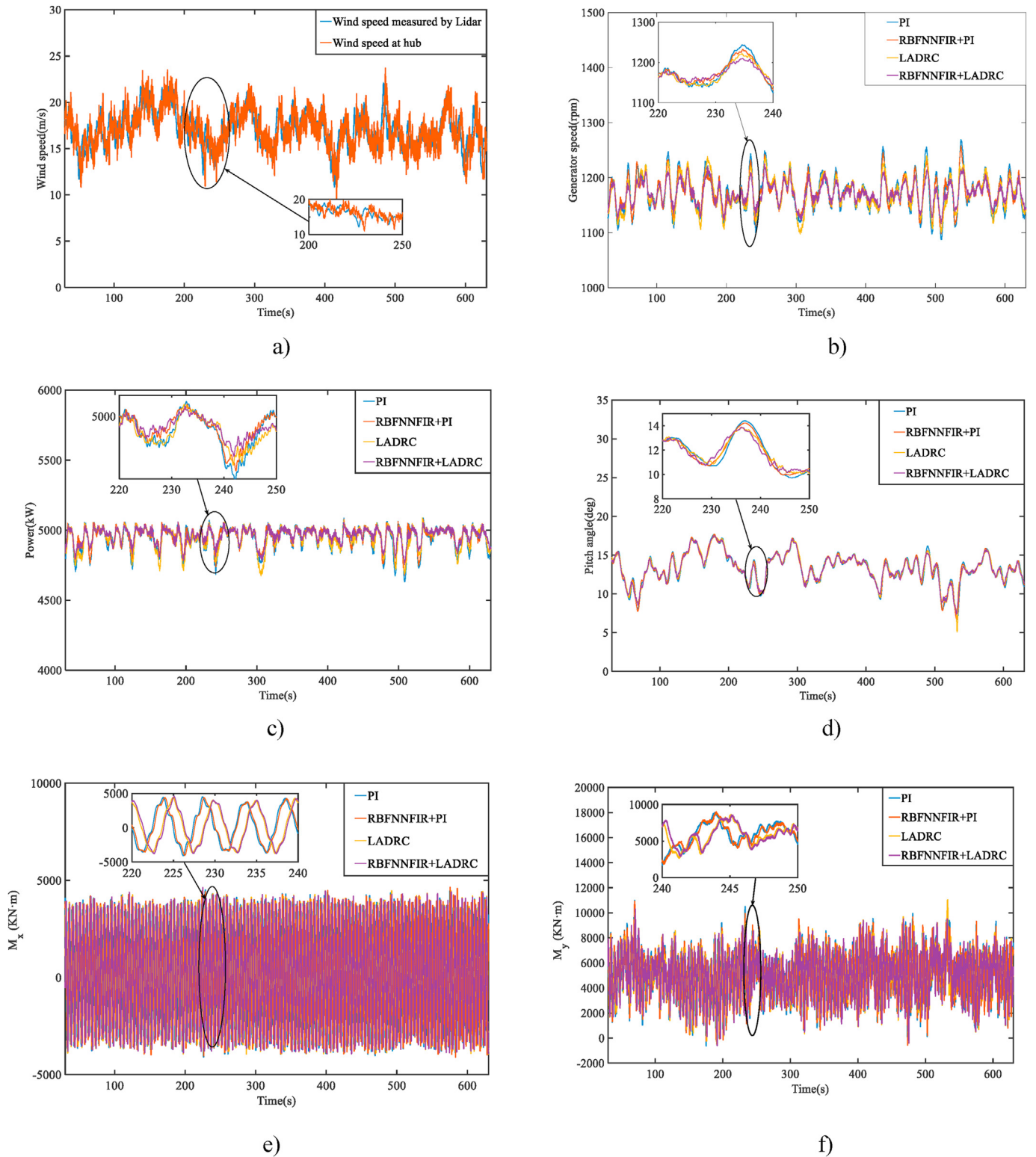
Fig. 12. Comparison of four control strategies under turbulent wind speed: a) Turbulent wind speed; b) Generator speed curve; c) Power curve; d) Pitch angle curve; e) Bladeroot moment M_x curve; f) Bladeroot moment M_y curve.

the traditional PI control, our proposed control strategy can reduce the mean value of blade root load moment in y direction by 0.35%, and the variance by 4.3%. The feedforward control loop is added and the LADRC control algorithm with stronger disturbance rejection is adopted, the better control effect is achieved in controlling the

generator speed and power fluctuation. Single feedback control is not as effective as feedforward and feedback compound control. Due to the advanced action of the pitch actuator, the fluctuation of moment in y direction of the blade root can be reduced.
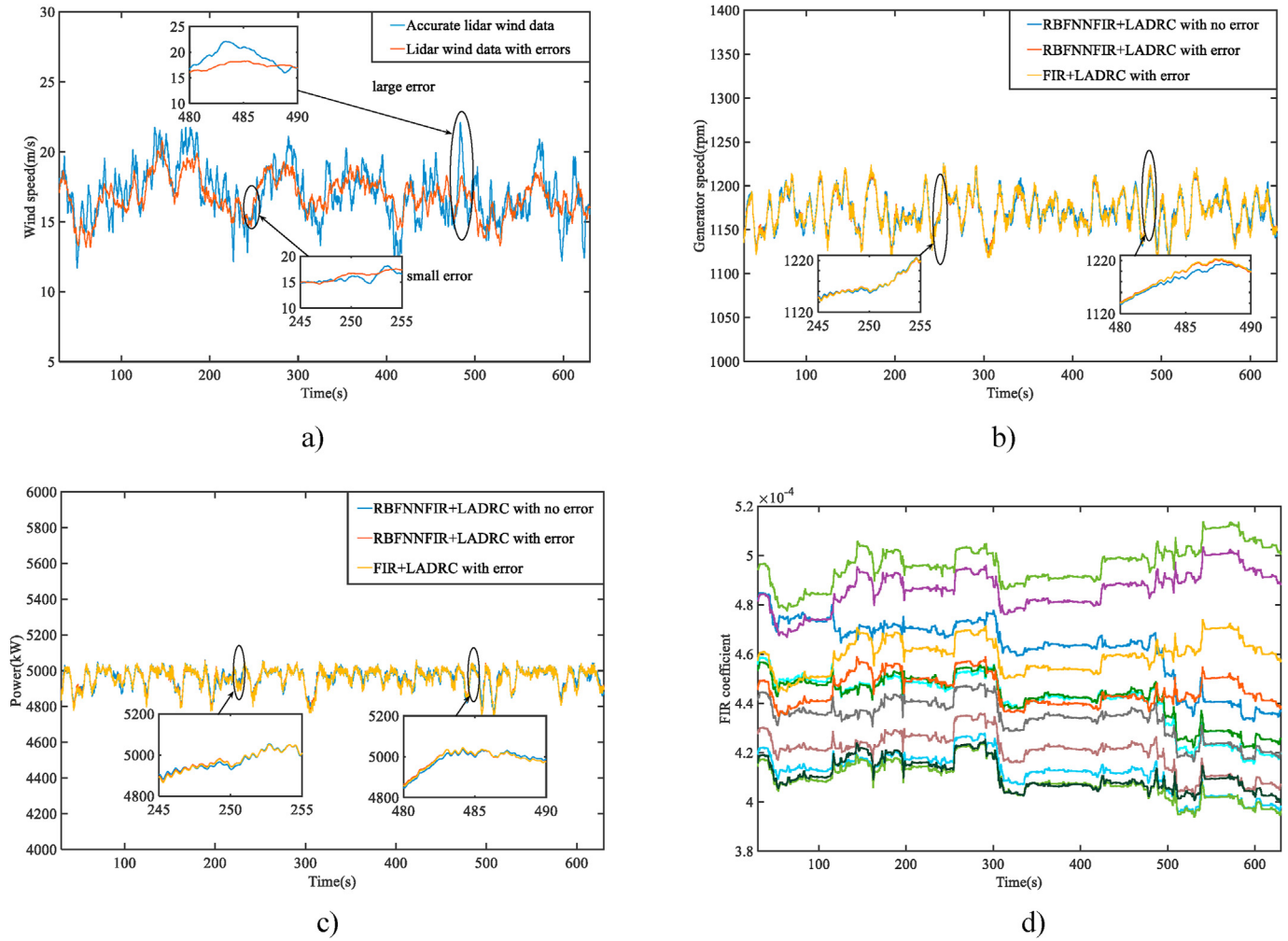
a)

b)

c)

d)

Fig. 13. Comparison of system control effect with measurement error: a) LIDAR measured wind speed; b) Generator speed curve; c) Power curve; d) Coefficient of FIR controller.
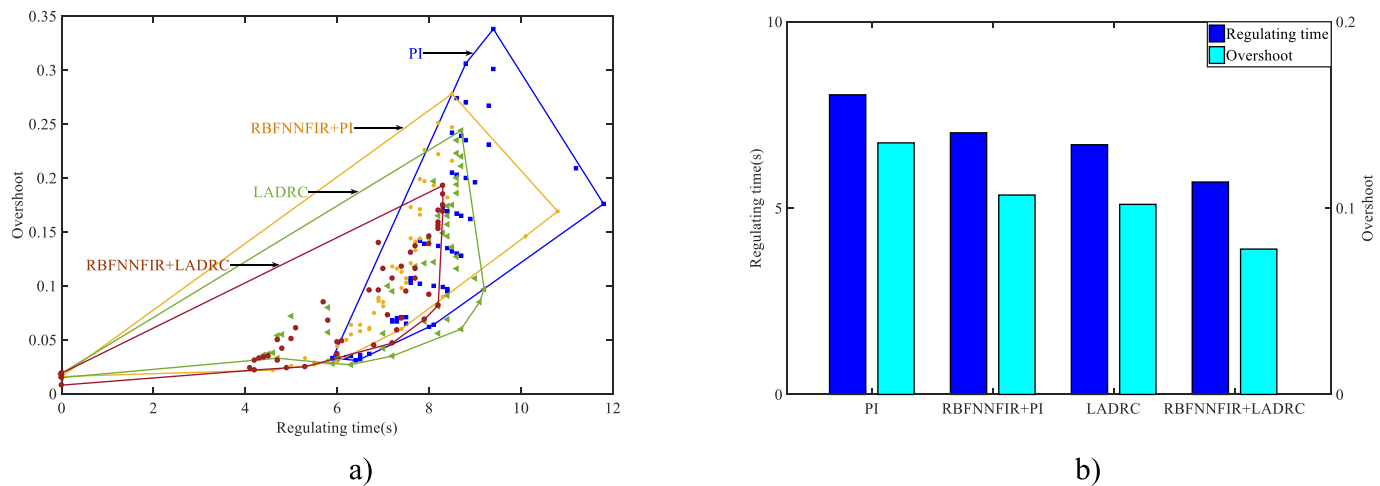

a)

b)

Fig. 14. Generator speed regulation time and overshoot analysis: a) Control indicators; b) Average statistics of indicators.

4.2. Experimental analysis of disturbance rejection and robustness

The fluctuation of wind speed can be regarded as the external disturbance of the pitch control system, while the measurement error of LIDAR is the internal disturbance. This part of experiment focuses on the anti-interference performance of the control algorithm to the internal disturbance. In order to assess the disturbance rejection of the RBFNNFIR + LADRC approach to the measurement error of LIDAR, the coefficients in Equation (8) are modified to simulate the measurement error of LIDAR. Two feedforward control

Table 4
Turbulent wind conditions.

Number	Turbulence model	Turbulence intensity	Mean wind speed (m/s)	Wind profile type	Lead time(s)
1	IECKAI	B	17	PL	2.9
2	IECVKM	B	17	PL	2.9
3	GP_LLJ	B	17	PL	2.9
4	NWTCUP	B	17	PL	2.9
5	SMOOTH	B	17	PL	2.9

algorithm are adopted, including fixed coefficient feedforward controller and RBFNNFIR feedforward controller. The statistics of the generator speed and power fluctuation show that the disturbances rejection of RBFNNFIR feedforward control system is stronger than the fixed coefficient feedforward controller.

Fig. 13 (a) - (c) show that when the measurement error of LIDAR is large, the fluctuation of generator speed and power will increase. Conversely, the fluctuation of speed and power will be close to the original with no measurement error. Through the statistical analysis of the data in Fig. 13 (b)–(c), the speed and power variance of fixed coefficient feedforward controller are 21.61 and 57.88, respectively. In contrast, the speed and power variance are 20.7 and 55.56 when RBFNNFIR feedforward controller is adopted, so RBFNNFIR can automatically adjust the coefficient of feed-forward controller as shown in Fig. 13 (d) to reduce the generator speed and power fluctuation, and the pitch control system disturbances rejection is stronger.

In order to measure the robustness of the pitch control system under step wind condition, we use two indexes commonly used in control: the adjustment time and the overshoot. We analyzed the generator speed stability adjustment time and overshoot with the different step wind speed respectively at different initial wind speeds. Fig. 14 (a) shows that the four control strategies can ensure the control stability under different step wind speed. Compared with each other, the control strategy proposed in this paper has an obvious downward trend in mean value of generator speed regulation time and overshoot, as shown in Fig. 14 (b), so the control robustness is better.

To test the robustness of the pitch control system under different turbulence wind condition, five turbulence models commonly used in TurbSim are adopted. According to IEC 61400-1 standard, the turbulence intensity level B is selected, as shown in Table 4. Table 5 presents the statistical analysis results of the maximum, minimum, mean and variance of speed and power, as well as the blade root load moment in x and y directions using four control strategies.

Table 5 depicts the change of each index under the four control strategies. The mean values of speed, power variance and the max blade root moment in x and y direction are significantly reduced, but the moment fluctuation in x direction has no obvious change. The mean and variance value of M_x under the four control strategies is basically the same. Fig. 15 depicts the results.

After calculation in Table 5, the mean value of the generator speed fluctuation, power fluctuation standard deviation and the max value of the blade root load moment in x direction under the variable gain PI control is 30.56, 74.46, 12552.38 kN m. Under the same setting, the mean value under the RBFNNFIR + LADRC control is 18.08, 49.62, 10148.38 kN m, the composite intelligent pitch control algorithm proposed in this paper can reduce the speed fluctuation by 40.8%, the power fluctuation by 33.4%, and the max load moment value of the blade root in x direction by 19.1%, and the max load moment value of the blade root in y direction by 7.2%. Due to the combination advantages of feedforward control and LADRC control algorithm, the composite intelligent pitch control algorithm

Table 5
Control index data of different control strategies under various wind conditions.

| Turbulence model	Control algorithm	ω_{max} (rpm)	ω_{min} (rpm)	ω_{mean} (rpm)	ω_{std}	P_{max} (kW)	P_{min} (kW)	P_{mean} (kW)	P_{std}	M_{x-max} (kNm)	M_{x-min} (kNm)	M_{x-mean} (kNm)	M_{x-std}	M_{y-max} (kNm)	M_{y-min} (kNm)	M_{y-mean} (kNm)	M_{y-std}
IECKAI	PI	1335.5	1067.3	1172.8	39.2	5129.5	4546.6	4934.1	96.2	5387.4	-4363.7	196.2	2530.4	14168.3	-977.9	5105.7	2104.5
	RBFNNFIR + PI	1282.6	1082.7	1172.6	28.8	5114.3	4611.9	4950.5	75.6	4802.6	-4241.2	185.5	2524.4	12314.5	-606.8	5096	1984.9
	LADRC	1314.7	1074.1	1170.8	32.8	5136	4575.5	4939.1	87.2	4663	-4272	195.6	2526.3	13908.1	-755.6	5083.3	2020
	RBFNNFIR + LADRC	1231.6	1079.6	1170.9	21.7	5077.6	4599	4958.2	63	4585.6	-4242.5	190.2	2526.1	10864.2	-707.2	5088.8	1915.8
IECVKM	PI	1377.8	1046.9	1172.9	47.2	5171.5	4459	4921.6	114.7	5812.23	-4617.4	198.8	2540.3	15133	-1286.3	5055.7	2196.2
	RBFNNFIR + PI	1293.4	1081.9	1172.5	32.7	5123.7	4608.9	4944.2	86.6	5095.5	-4524.5	183.3	2533.9	12026.7	-583.6	5045.5	2020.2
	LADRC	1308.3	1066.7	1169.8	39.2	5131.7	4544.2	4924.7	105.3	4795.2	-4305	196.7	2535.5	13513.8	-959	5025.4	2039.4
	RBFNNFIR + LADRC	1247	1082.1	1170.6	22.2	5088.7	4609.6	4957.3	65.8	4934.9	-4364.2	190	2535.2	10445.5	-1223.4	5047.8	1943.5
GP_LLJ	PI	1245.6	1123.2	1173.5	18.9	5059.4	4784.3	4968.3	46.1	4215.3	-3906.5	148.2	2499.1	9458.8	938.1	5108.1	1328.8
	RBFNNFIR + PI	1229.4	1133.2	1173.5	15.2	5053.6	4827.3	4974.8	38.2	4148.9	-3860	147.8	2499.8	9083.3	1126.2	5112.8	1306.3
	LADRC	1215.8	1128.4	1172.9	15.8	5041.8	4806.9	4971	40.5	4219.2	-3881.6	147.1	2502.8	8393.4	1004.7	5102.9	1277.9
	RBFNNFIR + LADRC	1213.1	1134.5	1173	13.3	5035.8	4832.9	4975.5	34.2	4165.6	-3883.1	147.6	2502.9	8413.8	1031.1	5107.2	1277.6
NWTCUP	PI	1173.4	1125.3	1173.4	24.7	5083.4	4738.4	4958.9	59.8	4311.7	-4161.4	176.9	2504.9	12954.9	-760.1	5146.4	1708.6
	RBFNNFIR + PI	1257.4	1116.9	1173.4	19.4	5069.5	4793.3	4967.6	48.4	4357.4	-4163.3	174.5	2505.3	12096.6	-398.1	5146.7	1668.7
	LADRC	1232.9	1123.2	1172.4	20.1	5054.7	4757.7	4963.8	51.2	4379	-4127.3	172.5	2507.1	11651.9	-866.7	5131.1	1641.7
	RBFNNFIR + LADRC	1227.7	1116.9	1172.6	17.3	5047.9	4784.9	4968.6	44.1	4313.8	-4095.5	172.8	2508.4	11281.2	-644.6	5134.8	1624.4
SMOOTH	PI	1259.4	1116.9	1173.5	22.8	5068.9	4758.2	4961.5	55.5	4327.8	-4081	162.5	2502.7	11046.9	136.9	5116.1	1547.3
	RBFNNFIR + PI	1240	1128.5	1173.3	18.2	5060	4806.8	4969.3	45.5	4344.2	-4043.7	161.7	2503.6	10547.4	501.3	5120	1518.2
	LADRC	1226	1122.9	1172.6	19.5	5046.2	4783.5	4964.3	50	4379.7	-4039.1	160.6	2504.2	9727.8	223.4	5107.4	1508.2
	RBFNNFIR + LADRC	1219.9	1133.2	1172.7	15.9	5041.6	4827.1	4970.4	41	4328.3	-3989.3	161.4	2505.4	9737.2	199.3	5115	1493.5
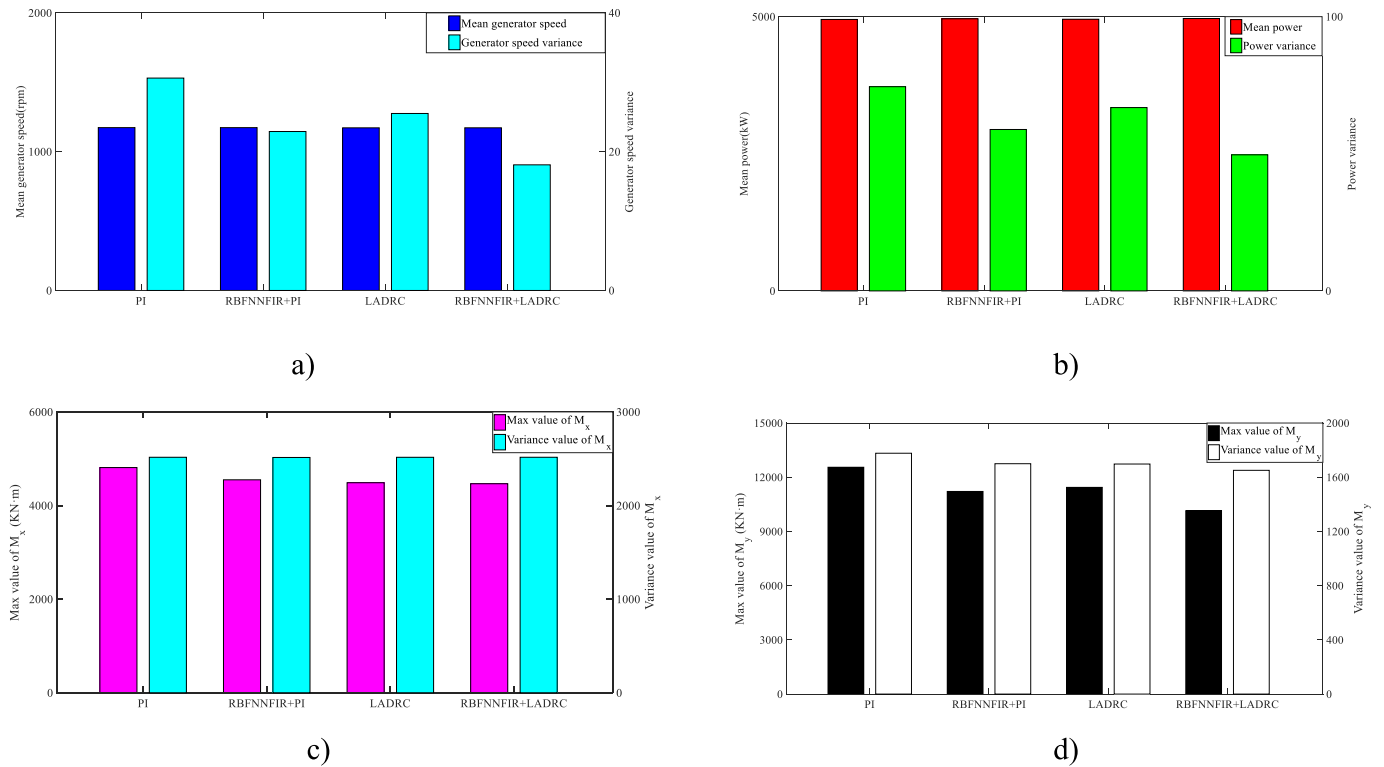
Fig. 15. Index analysis of generator speed, power and blade root load moment: a) Generator speed; b) Power; c) Load moment M_x; d) Load moment M_y.

proposed in this paper has the better control effect and the stronger robustness under the five turbulence wind conditions.

5. Conclusion and future work

Advanced LIDAR-based wind measurement technologies provide a novel approach to realizing intelligent wind turbine control. A feedforward controller can make full use of the wind speed data measured by LIDAR to ensure that when a wind speed fluctuation is sensed, a pitch actuator can act in advance, reducing the fluctuation of generator speed and power, and effectively reducing the max moment value of blade root. The adaptive intelligent control with variable parameters can dynamically adjust the controller's parameters according to different wind conditions, which enhances the disturbance rejection and robustness of the pitch control system.

In this paper, we develop a composite intelligent pitch control strategy to address the problem of poor disturbance rejection and adaptability of pitch control system. We use RBFNN to realize the function approximation between the feedforward pitch control quantity and the generator speed error. Through the Jacobian matrix information, the coefficients of the FIR controller are modified, so that the RBFNNFIR control algorithm can adjust the coefficient intelligently and adaptively according to the wind speed fluctuation. By analysing the distribution of poles and zeros of the closed-loop system under different wind speed, the relationship between pitch angle and the observation bandwidth of ESO is obtained, which enhances the adaptability of LADRC controller. Initial results, based on the analysis of simulation experimental data under different wind conditions, show that the composite intelligent pitch control strategy can reduce a generator speed fluctuation by about 40.8%, the power fluctuation by about 33.4%, the max torque value of the blade root in *x* direction by about 19.1%, and the max moment value of the blade root in *y* direction by about 7.2%.

In the future, we will use PLC programming language to realize the control algorithm proposed in this paper, and solve the engineering problems in PLC hardware configuration, it will realize the wind turbine optimizing control. The development of full wind speed range control algorithm based on LIDAR will further improve the wind energy utilization of wind turbine, LIDAR can also be applied to yaw control, taking the advantage of measurement accuracy to improve the power generation. With the growth of wind turbine unit capacity, load reduction will be the top priority of wind turbine control, which is related to the safe and stable operation of wind turbine.

CRediT authorship contribution statement

Chengzhen Jia: Data curation, Methodology, Writing - original draft, preparation, Software. **Lingmei Wang:** Resources, Conceptualization. **Enlong Meng:** Visualization. **Liming Chen:** Writing - review & editing. **Yushan Liu:** Software, Validation. **Wenqiang Jia:** Supervision. **Yutao Bao:** Project administration. **Zhenguo Liu:** Writing - review & editing.

Declaration of competing interest

The authors declare that they have no known competing financial interests or personal relationships that could have appeared to influence the work reported in this paper.

Acknowledgement

References

[1] P. Enevoldsen, G. Xydis, Examining the trends of 35 years growth of key wind turbine components, Energy Sustain. Dev. 50 (2019) 18–26, https://doi.org/10.1016/j.esd.2019.02.003.

[2] Y. Yuan, X. Chen, J. Tang, Multivariable robust blade pitch control design to reject periodic loads on wind turbines, Renew. Energy 146 (2020) 329–341, https://doi.org/10.1016/j.renene.2019.06.136.

[3] J. Bao, M. Wang, H. Yue, et al., Pseudo-LIDAR data analysis and feed-forward wind turbine control design 48 (8) (2015) 483–488, https://doi.org/10.1016/j.ifacol.2015.09.014. IFAC-Papers OnLine.

[4] A. Scholbrock, P. Fleming, D. Schlipf, et al., Lidar-enhanced wind turbine control: past, present, and future, in: 2016 American Control Conference (ACC), IEEE, 2016, https://doi.org/10.1109/ACC.2016.7525113.

[5] F. Haizmann, D. Schlipf, S. Raach, et al., Optimization of a feed-forward controller using a CW-lidar system on the CART3, Proc. Am. Contr. Conf. 2015 (2015) 3715–3720, https://doi.org/10.1109/ACC.2015.7171907.

[6] N. Wang, K.E. Johnson, A.D. Wright, FX-RLS-Based feedforward control for LIDAR-enabled wind turbine load mitigation, IEEE Trans. Contr. Syst. Technol. 20 (5) (2012) 1212–1222, https://doi.org/10.1109/TCST.2011.2163515.

[7] V. Rezaei, LIDAR-based robust wind-scheduled control of wind turbines[C], in: 2014 American Control Conference(ACC) 2014, IEEE, 2014, https://doi.org/10.1109/ACC.2014.6859395.

[8] B. Han, L.W. Zhou, Z. Zhang, LIDAR-assisted radial basis function neural network optimization for wind turbines, IEEJ Trans. Electr. Electron. Eng. (1) (2018), https://doi.org/10.1002/tee.22514.

[9] M. Mirzaei, M. Soltani, N.K. Poulsen, et al., An MPC approach to individual pitch control of wind turbines using uncertain LIDAR measurements, in: Proceedings of European Control Conference, IEEE, Zurich, 2013, pp. 490–495, https://doi.org/10.23919/ECC.2013.6669729.

[10] M. Mirzaei, M.H. Hansen, A LIDAR-assisted model predictive controller added on a traditional wind turbine controller, in: 2016 American Control Conference (ACC), IEEE, 2016, https://doi.org/10.1109/ACC.2016.7525110.

[11] D. Schlipf, L.Y. Pao, P.W. Cheng, Comparison of feedforward and model predictive control of wind turbines using LIDAR, in: 51st IEEE Conference on Decision and Control, IEEE, 2012, https://doi.org/10.1109/CDC.2012.6426063.

[12] D. Schlipf, P. Grau, S. Raach, et al., Comparison of linear and nonlinear model predictive control of wind turbines using LIDAR, in: American Control Conference, IEEE, 2014, https://doi.org/10.1109/ACC.2014.6859205.

[13] Colombo L, Corradini, Maria L, et al. Pitch angle control of a wind turbine operating above the rated wind speed: a sliding mode control approach[J]. ISA (Instrum. Soc. Am.) Trans.. DOI:10.1016/j.isatra.2019.07.002.

[14] A. Amirhossein, S. Reza, J. Ali, Performance and robustness of optimal fractional fuzzy PID controllers for pitch control of a wind turbine using chaotic optimization algorithms, ISA (Instrum. Soc. Am.) Trans. 79 (2018) 27–44, https://doi.org/10.1016/j.isatra.2018.04.016.

[15] R. Gao, Z. Gao, Pitch control for wind turbine systems using optimization, estimation and compensation, Renew. Energy 91 (2016) 501–515, https://doi.org/10.1016/j.renene.2016.01.057.

[16] Y. Yuan, J. Tang, Adaptive pitch control of wind turbine for load mitigation under structural uncertainties, Renew. Energy 105 (2017) 483–494, https://doi.org/10.1016/j.renene.2016.12.068.

[17] M.A. Abdelbaky, X.J. Liu, D. Jiang, Design and implementation of partial offline fuzzy model-predictive pitch controller for large-scale wind-turbines, Renew. Energy 145 (2020) 981–996, https://doi.org/10.1016/j.renene.2019.05.074.

[18] Y. Ren, L. Li, J. Brindley, et al., Nonlinear PI control for variable pitch wind turbine, Contr. Eng. Pract. 50 (2016) 84–94, https://doi.org/10.1016/j.conengprac.2016.02.004.

[19] A. Lasheen, M.S. Saad, H.M. Emara, et al., Continuous-time tube-based explicit model predictive control for collective pitching of wind turbines, Energy 118 (2017) 1222–1233, https://doi.org/10.1016/j.energy.2016.11.002.

[20] A. Asgharnia, A. Jamali, R. Shahnazi, et al., Load mitigation of a class of 5-MW wind turbine with RBF neural network based fractional-order PID controller, ISA (Instrum. Soc. Am.) Trans. (2019), https://doi.org/10.1016/j.isatra.20.

[21] H. Jafarnejadsani, J. Pieper, Gain-Scheduled l_1-optimal control of variable-speed-variable-pitch wind turbines, IEEE Trans. Contr. Syst. Technol. 23 (1)

[22] Y.Q. Zhang, D.H. Li, Z.Q. Gao, et al., On oscillation reduction in feedback control for processes with an uncertain dead time and internaleexternal disturbances, ISA (Instrum. Soc. Am.) Trans. 59 (2015) 29–38, https://doi.org/10.1016/j.isatra.2015.08.002.

[23] Z.L. Wu, D.H. Li, Y.L. Xue, et al., Gain scheduling design based on active disturbance rejection control for thermal power plant under full operating conditions, Energy 185 (2019) 744–762, https://doi.org/10.1016/j.energy.2019.07.077.

[24] J.M. Jonkman, S. Butterfield, W. Musial, et al., Definition of a 5MW reference wind turbine for offshore system development[R], in: Office of Scientific & Technical Information Technical Reports, 2009.

[25] A. Amirhossein, S. Reza, J. Ali, Performance and robustness of optimal fractional fuzzy PID controllers for pitch control of a wind turbine using chaotic optimization algorithms, ISA (Instrum. Soc. Am.) Trans. 79 (2018) 27–44, https://doi.org/10.1016/j.isatra.2018.04.016.

[26] A. Asgharnia, A. Jamali, R. Shahnazi, A. Maheri, Load mitigation of a class of 5-MW wind turbine with RBF neural network based fractional-order PID controller, ISA (Instrum. Soc. Am.) Trans. (2019), https://doi.org/10.1016/j.isatra.2019.07.006.

[27] R.F. Nayeh, H. Moradi, G. Vossoughi, Multivariable robust control of a horizontal wind turbine under various operating modes and uncertainties: a comparison on sliding mode and H∞ control, Int. J. Electr. Power Energy Syst. 115 (2020) 105474, https://doi.org/10.1016/j.ijepes.2019.105474.

[28] G. Kavari, M. Tahani, M. Mirhosseini, Wind shear effect on aerodynamic performance and energy production of horizontal axis wind turbines with developing blade element momentum theory, J. Clean. Prod. 219 (2019) 368–376.

[29] W. Liu, C. Li, Y. Liu, et al., Predictive control of wind turbine for load reduction during ramping events, Int. J. Electr. Power Energy Syst. 93 (2017) 135–145, https://doi.org/10.1016/j.ijepes.2017.05.025.

[30] M. Harris, M. Hand, A. Wright, Lidar for turbine control: March 1, 2005 - November 30, 2005[R], in: National Renewable Energy Laboratory Technical Reports, 2006.

[31] Nacelle-based wind LIDAR product information Manual[DB/OL]. http://www.movelaser.com/madmin/upload/file/MolasNL_Whitepaper.pdf.

[32] E. Simley, L.Y. Pao, N. Kelley, et al., LIDAR wind speed measurements of evolving wind fields, in: Aiaa Aerospace Sciences Meeting, 2012, https://doi.org/10.2514/6.2012-656.

[33] Darko Vrečko, Marko Nerat, Damir Vrančić, et al., Feedforward-feedback control of a solid oxide fuel cell power system, Int. J. Hydrogen Energy 12 (43) (2018) 6352–6363, https://doi.org/10.1016/j.ijhydene.2018.01.203.

[34] R. Jeyasenthil, S.B. Choi, Harsh Purohit, et al., Robust position control and disturbance rejection of an industrial plant emulator system using the feedforward-feedback control, Mechatronics 57 (2019) 29–38, https://doi.org/10.1016/j.mechatronics.2018.11.004.

[35] J.S. Vipperman, R.A. Burdisso, Adaptive feedforward control of non-minimum phase structural systems, J. Sound Vib. 183 (3) (1995) 369–382, https://doi.org/10.1006/jsvi.1995.0260.

[36] N. Wang, LIDAR-assisted Feedforward and Feedback Control Design for Wind Turbine Tower Load Mitigation and Power Capture enhancement[D], Colorado School of Mines, 2013.

[37] G.J. Li, Adaptive PID Control Based on RBFNN Identification[D], Southwest Jiaotong University, Chengdu, 2005.

[38] D.L. Yang, Z.M. Liu, Misadjustment analysis and improvement of BP algorithms for multilayer forward neural networks, Acta Electron. Sin. 23 (1) (1995) 117–120.

[39] J.Q. Han, Active Disturbance Rejection Control Technique—The Technique for Estimating and Compensating the uncertainties[M], National Defense Industry Press, 2008.

[40] Z.Q. Gao, Scaling and bandwidth-parameterization based controller tuning, in: Proceedings of the 2003 American Control Conference 6, 2003, pp. 4989–4996, https://doi.org/10.1109/ACC.2003.1242516.

[41] Wind turbine design software–Bladed[DB/OL]. https://www.dnvgl.com/services/wind-turbine-design-software-bladed-3775.

[42] FAST v8[DB/OL]. https://nwtc.nrel.gov/FAST8.